Issue VI, 22 November 2023
e-ISSN 2707-9481 Institute of Metallurgy and Ore Beneficiation, Satbayev University, Almaty, Kazakhstan
ISBN 978-601-323-356-7 https://doi.org/10.31643/2023.27

Abdulla Khursanov
PhD, Senior Researcher, Chairman of the Board of Almalyk MMC JSC
E-mail: info@agmk.uz
Republic of Uzbekistan

Abdurashid Hasanov
DSc, Professor, Deputy Chief Engineer for science of Almalyk MMC JSC
E-mail: abdurashidsoli@mail.ru
Republic of Uzbekistan

Behzod Tolibov
Doctor of Technical Sciences, Professor,
Innovative Development Agency
E-mail: b.tolibov@mininnovation.uz
Republic of Uzbekistan

Physical Properties of Liquid Slag, their Influence on the Basic Parameters of Technological Processes

Abstract: In this article given physical properties of liquid slag, their influence on the basic parameters of technological processes in Almalyk mining and metallurgical plant. The physical properties of melts directly affect the main parameters of pyrometallurgical processes, as well as the design and operation features of equipment. The physical properties of melts (F) are functions of the composition of the phase under study (Xij) and external parameters that determine the state of the system. These properties reflect the structure of the melt, i.e., they are structure-sensitive properties. The physical properties of the liquid phase should also be understood as its properties that are not associated with changes in its material composition or chemical properties, or are associated to an insignificant extent.

Keywords: slag, matte, copper, temperature, density, viscosity, surface layer, electrical conductivity, interfacial properties, double electrical parameters, crystallization, thermal conductivity, separation, smelting, furnace.

Cite this article as: Khursanov A., Hasanov A., Tolibov B. (2023). Physical Properties of Liquid Slag, their Influence on the Basic Parameters of Technological Processes. *Challenges of Science*. Issue VI, 2023, pp. 225-232. https://doi.org/10.31643/2023.27

Introduction

The physical properties of melts directly affect the main parameters of pyrometallurgical processes, as well as the design and operation features of equipment. The physical properties of melts (F) are functions of the composition of the phase under study (Xij) and external parameters that determine the state of the system. These properties reflect the structure of the melt, i.e., they are structure-sensitive properties. The physical properties of the liquid phase should also be understood as its properties that are not associated with changes in its material composition or chemical properties, or are associated to an insignificant extent (Yessengaliyev et al., 2022).

The distinction between physical and chemical properties is quite arbitrary, since physical properties, as mentioned earlier, are functions of the chemical composition.

The relationship between physical properties and chemical composition is quite complex and in most cases cannot be calculated theoretically, so experimental methods are usually used to determine it. Physical properties (F_1) can be related to one phase (j)

$$F_1 = F_1(X_{ij}) \quad (1)$$

Where, *1* is the index of properties, so to interphase interaction in the absence of material exchange between phases

$$F = F(X_{ij\#1} \cdot X_{ij\#2 \ldots\ldots} X_{ij\#n}) \quad (2)$$

Physical properties and the interaction of two phases: interfacial electrical layer, etc. are of practical importance.

If the j-th phase consists of m components, i.e. (I = 1.2…….m), then if the condition is met

$F(X_{ij}) = \sum_{i=1}^{i=m} X_{ij}F_1$ (3)

$\sum X_{ij} = 1$ (4)

where F_{1i} is a similar property of the i-th component of property F, which is additive with respect to the component composition.

To establish additivity, it is necessary to correctly select the method of expressing the value of the property and its dimension. For example, in a number of cases, the density of liquid slags is additive with respect to the density of the components included in them, if these densities are presented in the form of molar volumes with the appropriate dimension.

Additivity conditions can also be written as

$\frac{\partial F(X_{ij})}{\partial X_{ij}} = F_{1ij} = C, \;\; C = const$ (5)

In most cases, additivity is not observed. Methods for analytical and graphical representation of "composition-property" relationships are given earlier and will be used further to illustrate the most important properties of slags depending on their composition.

The most important properties are: dependence of the state of aggregation on temperature, density, viscosity, surface layer, electrical conductivity, interfacial properties, double electrical parameters. These properties are the most important; then the hedgehogs significantly influence the technological process and the design of the equipment used. They determine the speed of phase separation, the durability of refractories, the dimensions of the melting unit, the process temperature and much more. The most important physical properties of melts will be discussed in detail later in this section.

However, there are other physical properties that can be divided into two groups:

– physical properties, the influence of which on technology and equipment is known and the values of these properties are used in technological and structural calculations.

– physical properties, the influence of which on the technological process has not been established or is absent.

The first group includes such properties as thermophysical (thermal conductivity, degree of surface emissivity, etc.), parameters of diffusion, heat content, heat capacity, etc.

The second group includes: radioactivity, radiation permeability and parameters of interaction with ionizing radiation, magnetic properties, acoustic properties.

However, the lack of information about the practical use of the properties of the second group does not mean that their use is impossible. Thus, in the literature there is information about attempts to use acoustic or magnetic treatment to disrupt the stability of separation dispersoids and intensify the processes of coarsening of fine suspended matter (Shmonin, 1981; Vanyukov & Zaitsev, 1967; Kenzhaliyev, 2019).

In ferrous metallurgy, MHD separation systems are being developed to separate metal from blast furnace and open-hearth slags.

The electrical conductivity of slags was not of interest for practical metallurgy for a long time, but became a very important parameter from the moment when the use of electrothermal furnaces began for melting raw materials and depleting slags.

The parameters of the interaction of liquid metals with a magnetic field were of purely academic interest until the use of induction furnaces began.

Therefore, if a physical property is not used in black copper production processes, this does not mean that it will not be used in the future.

State diagrams of slag systems. Phase diagrams of slag systems characterize their phase state at each given point of the general composition. The phase diagrams include composition-dependent temperatures of the beginning and end of crystallization F_1 and F_2.

$F_1=F^l$ (temperature at the liquidus line),

$F_2=F^s$ (temperature at the solidus line),

$F=F(X_i^0)$,

Where, $\{X_i^0\}$ - set of concentrations of components reflecting the initial state of the system. In the literature there are diagrams of the state of slag systems of various compositions. If they are given in weight fractions (percentages), then they require conversion to mole fractions for ease of use. In the case of using a unified notation system, Musical conversion formulas are used. For a given initial state, it is possible to

determine the equilibrium compositions and the ratio of liquid and solid phases in the temperature range, the temperature of the beginning and end of crystallization.

This means that the state diagram can be used to establish a dependency

$$M_j = F_j(X_j^0 TP) \quad (6)$$

$$X_{ij} = F_{ij}(X_i^0 TP) \quad (7)$$

Analytically, any function, even a discontinuous one, can be represented using the methods of modern mathematics in the form of a set of known functions, with any predetermined degree of accuracy.

The set of known functions is an approximating function. However, the use of classical mathematical apparatus is difficult due to the great complexity of approximating functions for real systems. Until recently, the use of such functions was almost impossible due to purely mathematical difficulties and computational complexity. Therefore, only the analytical expression for the dependence $F^l\{X_{ij}\}$ for limited regions of the phase diagram has received some development. The delimitation of regions, as a rule, is carried out along closed contours, including at the boundary, but not containing inside, figurative points corresponding to the compositions of the eutectics and the crystallization line. In this case, the approximation formulas are much simpler.

Another difficulty that often prevents the use of the full approximation principle is the lack of data on individual areas of the system.

Therefore, in most cases, graphical methods for determining the state of systems are still used: state diagrams. One significant assumption must be made here. Currently, there is a huge database in the form of state diagrams of binary, triple and more complex systems. The development of modern mathematics and computer technology makes it possible to turn any graphic information into digital information and back. Even formal scanning from a drawing or drawing without user intervention.

The state diagrams in the computer memory are already recorded in digital form. The development of digital technologies allows us to hope that they are able to replace analytical approximation methods and be used to perform technological calculations. In this case, the user can have at his disposal both illustrative and graphic material and the ability to analyze it by computer construction of partial dependencies and their graphs for given variables and intervals.

In accordance with the previous section, their molar concentrations will be designated as $X_{2.3}$ and $X_{5.3}$, respectively. The molar contents of the elements Cu, Fe, S, O are designated as $X_{1.3}$, $X_{4.3}$, $X_{19.3}$, $X_{24.3}$ and FeO and Fe_3O_4 as $X_{6.3}$ and $X_{7.3}$, respectively.

If the phase diagram uses the weight fractions of components in percent (%), then they are designated as $X^в_{ij}$ and are converted into X_{ij} according to a known ratio.

Analysis of binary phase diagrams shows that the FeS-FeO system is homogeneous with a FeS content of more than 50% over the entire operating temperature range. The Cu_2S-FeS system is homogeneous at any composition at temperatures above 1423˚K.

Let us give a description of the liquidus surface of this system as interpreted by the author. A significant area of the liquidus surface is occupied by the field of primary crystallization of FeO by monotectic reactions

$L_{FeO} - FeO_s + L_S$.

The critical point of this zero is shifted from the center towards Cu_2S-FeS and has a composition of 50% Cu_2S, 27% FeO, 23% FeS and a temperature of 1165˚C.

The conodes, constricting the compositions of equilibrium coexisting sulfide and oxide melts formed as a result of the stratification of the oxysulfide melt, have a fan-shaped course from compositions concentrated in Cu_2S towards FeS-FeO. As the temperature increases, the delamination area shrinks. The temperature of the triple point E is 850˚C and is consistent with the work data [3].

The main conclusion from the above data is that the factor determining the nature of separation in the homogeneous FeS-FeO system is the presence of the third component Cu2S.

The data from both of the above phase diagrams can be used to determine the melting points and crystallization points in oxygen-containing and metallized mattes.

Naturally, these parameters will differ somewhat from the crystallization parameters characteristic of industrial mattes due to the presence of other components and contain iron both in the form of FeO and Fe_3O_4.

The state diagrams of slag systems are much more complex than matte systems. A common complication is the presence of iron in di- and trivalent forms. We accept the following notations for the main components of slag and their contents:

$(FeO)_i = \{_{6.4}$; $(Fe_3O_4)_i = X_{7.4}$; $(Fe_2O_3)i = X_{8.4}$; (8)

$(SiO_2)_i = \{_{11.4}$; $(CaO)_i = X_{12.4}$; $(Al_2O_3)i = X_{13.4}$; (9)

In equilibrium with the slags characteristic of copper production processes, there may be separate solid phases based on magnetite or silicon dioxide with their content of $X_{7.5}$ and $X_{11.6}$, respectively.

In non-ferrous metallurgy, iron-silicate slags are mainly used, the main components of which are iron and silicon oxides, and in some new processes, ferrite-calcium slags, the main components of which are iron and calcium oxides. Ferrous metallurgy slags (blast furnace, open hearth) occupy an intermediate position. Melting the slag does not always immediately lead to its fluidity. Due to the need for disaggregated silicon-oxygen complexes, the number and complexity of which increases with increasing SiO2, in the slag (X11.4), overheating of the slag is necessary. For slags with a high SiO2 content, the overheating temperature can reach hundreds of degrees. For highly basic ferrite-calcium slags, the overheating temperature is minimal; for other slags it has an intermediate value. The viscosity of slags also increases from ferrite-calcium slags to iron-silicate slags with a high content of silicon dioxide. These issues will be discussed in detail below. As for the questions of mathematical description of the properties of the corresponding slag, they are similar to those that were outlined for mattes.

The difference is that the phase diagram of slag systems is much more complex than the phase diagram of matte systems.

Thus, the basic binary state diagrams of slags are the state diagrams (FeO –SiO_2) ($X^B_{6.4} - X^B_{11.4}$); (FeO - CaO) ($X^B_{6.4} - X^B_{12.4}$); (SiO_2 – CaO) ($X^B_{11.4} - X^B_{12.4}$).

The first phase diagrams were obtained in equilibrium with gamma iron in relation to ferrous metallurgy. Highly reduced slags practically do not contain Fe^{3+}, therefore the content of Fe_3O_4 and Fe_2O_3 was not taken into account. On the other hand, slags with a high Fe^{3+} content were studied, obtained by smelting in the gas phase, which is air.

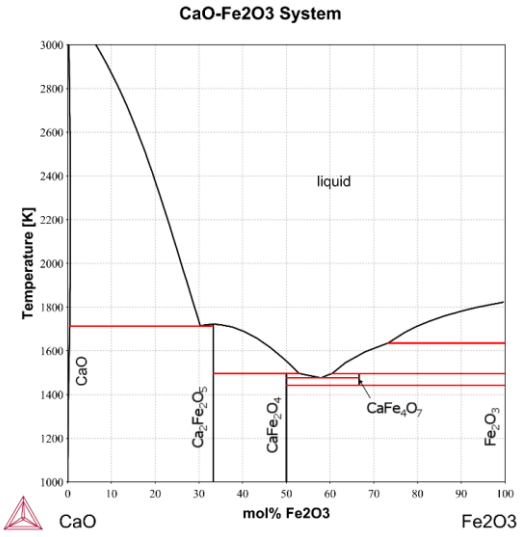

Fig.1. State diagram CaO – Fe_2O_3

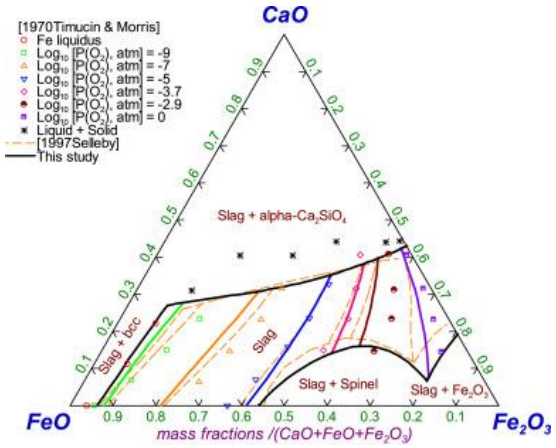

Fig. 2 State diagram CaO – FeO – Fe_2O_3 $(X^B_{12.4} - X^B_{6.4} - X^B_{8.4})$

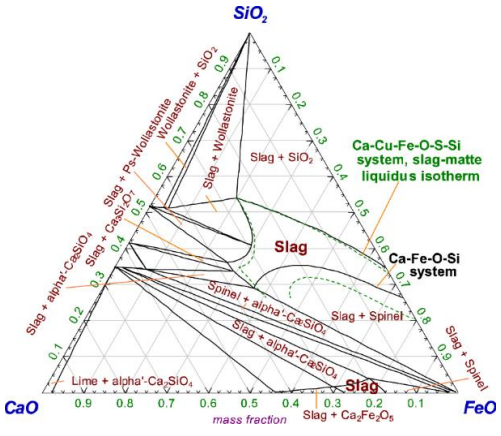

Fig.3. (1) State diagram (CaO – FeO – SiO_2) $(X^B_{12.4} - X^B_{6.4} - X^B_{11.4})$

In this case, the state diagram is of particular interest (Fe_2O_3 - CaO) ($X^B_{8.4} - X^B_{12.4}$), shown in Fig 1.

Non-ferrous metallurgy slags are closest to the FeO - SiO_2 system. There are two chemical compounds in this system: fayalite Fe_2SiO_4 and iron metasilicate $FeSiO_3$ (Vanyukov & Zaitsev, 1967). In the phase diagram obtained by other researchers (Shmonin, 1981) (according to scientists from Germany), the presence of iron

metasilicate is not confirmed, although in other respects it is similar to Selivanov's diagram (Vanyukov & Zaitsev, 1967; Hasanov, 2003).

For a better understanding of the melting and crystallization processes, it is necessary to consider ternary phase diagrams.

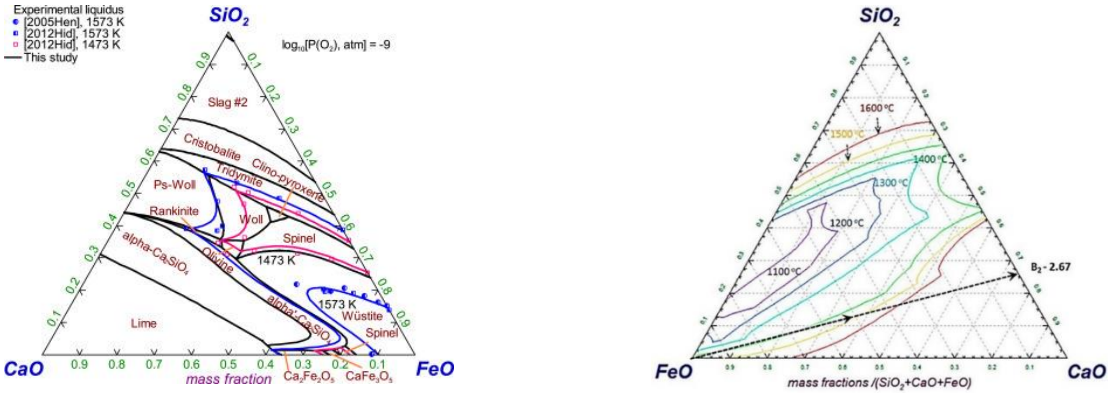

Fig. 3 (2). State diagram (CaO – FeO – SiO_2) $(X^{B}_{12.4} - X^{B}_{\mathbf{6.4}} - X^{B}_{\mathbf{11.4}})$

The state diagram is of some interest, (CaO-FeO-Fe_2O_3) $X_{12.4}$ - $X_{6.4}$ -$X_{8.4}$ shown in Fig.2.

This phase diagram also shows the partial pressure of oxygen (Po_2). From this diagram it can be seen that although the melting temperature increases with the replacement of FeO by Fe_2O_3, it does not increase very much. The dependence of Po_2 on composition is such that it allows the reduction of some oxides to metals. As a result of this, it is possible to obtain copper-poor slags over high-calcium ferritic slags, but this issue is beyond the scope of this section.

Next, consider two ternary state diagrams (CaO-FeO- SiO_2) **(**$X_{12.4}$ - $X_{6.4}$ -$X_{11.4}$) и (CaO - Fe_2O_3- SiO_2) ($X_{12.4}$ – $X_{8.4}$ -$X_{11.4}$) according to (Tsukihashi & Kimura, 2000).

These state diagrams are shown in Fig.3 and 4. Fig.5 shows the state diagram (FeO - Fe_2O_3 - SiO_2) ($X_{6.4}$ – $X_{2.4}$ -$X_{11.4}$).

From these diagrams it is possible to obtain approximate data for a system with different Fe^{3+}/Fe^{2+} ratios. Copper production slags are characterized by a low content of Fe^{3+} and CaO and can be considered within the framework of these phase diagrams (Hidayat et al., 2017).

The introduction of additional oxides (Al_2O_3) $X_{13.4}$, as well as (MgO, Na_2O, K_2O, MnO, etc.) into the system leads to the consideration of quaternary, quintuple and sixfold state diagrams. Even their graphic representation is associated with a number of difficulties, and working with graphic data is much more difficult than with state diagrams of two-component and three-component systems. The simplest method is the following: X_{ij} is fixed for the 1st additional component. Then a state diagram is drawn up from the condition

$$\sum_{j}^{i=3} X_{ij} = 1 - X_{ij} \qquad (10)$$

For example, you can imagine a state diagram ($X^{B}_{11.4}$ – $X^{B}_{12.4}$ -$X^{B}_{6.4}$) (CaO – FeO – SiO_2) при $X^{B}_{13.4}$ (Al_2O_3) = 10%.

Then $X^{B}_{11.4}$ - $X^{B}_{12.4}$ -$X^{B}_{6.4}$ = 90%.

Such triple state diagrams are sections of the general quadruple state diagram along a flat plane $X^{B}_{13.4}$ = 10%. There are quite a lot of fragments of such state diagrams in the literature.

Within the framework of this approach, we can consider the quaternary phase diagram (CaO - FeO - Fe_2O_3 - SiO_2) ($X_{11.4}$ - $X_{6.4}$ - $X_{8.4}$ - $X_{12.4}$), obtained in equilibrium with g-iron under isothermal conditions of 1450°C and 1550°C and changing the weight fraction of SiO_2 from 0 to 30%. This diagram shows only phase boundaries under isothermal conditions and oxygen partial pressures. However, such state diagrams are of significant interest for further use.

State diagrams ($X_{11.4}$- $X_{6.4}$ - $X_{8.4}$- $X_{12.4}$) (CaO - FeO - Fe_2O_3- SiO_2) are shown in Fig. 6 for the indicated supplied temperatures (Tsukihashi & Kimura, 2000).

Analysis of the phase diagram of slag systems makes it possible to determine the composition and phase ratio in a single association during slag crystallization, as well as to estimate the melting temperature (liquidus) and the end of crystallization (solidus). From the phase diagram, the composition of isolated compounds and eutectics can be determined.

In accordance with the work of the school of N.S. Kurnakov, the smoothness diagram can be used to judge the presence and, to some extent, dissociation of a chemical compound. If on a binary smoothness diagram the liquidus line has a common tangent at the top for common branches, then this indicates almost complete dissociation of the compound in the molten state. If the top of the maximum was formed by two branches of the liquidus line and there is a discontinuity in the derivative $\partial T/\partial X$, then this indicates a slight dissociation. A measure of the strength of chemical compounds is the angle between the tangents at the maximum point. This thermodynamic situation is depicted in Figure 1.

In the first case $\partial T/\partial X_+ = \partial T/\partial X_- = 0$.

In the second case $\partial T/\partial X_+ \neq \partial T/\partial X$ and have different signs. A measure of the strength of connected lines is either the value of the angle α between the tangents, or

$$K_\Sigma = K_1 + K_2 = |\partial T/\partial X_+| + |\partial T/\partial X_-| \qquad (11)$$

There are other possibilities for obtaining information using a state diagram, but they are beyond the scope of this section.

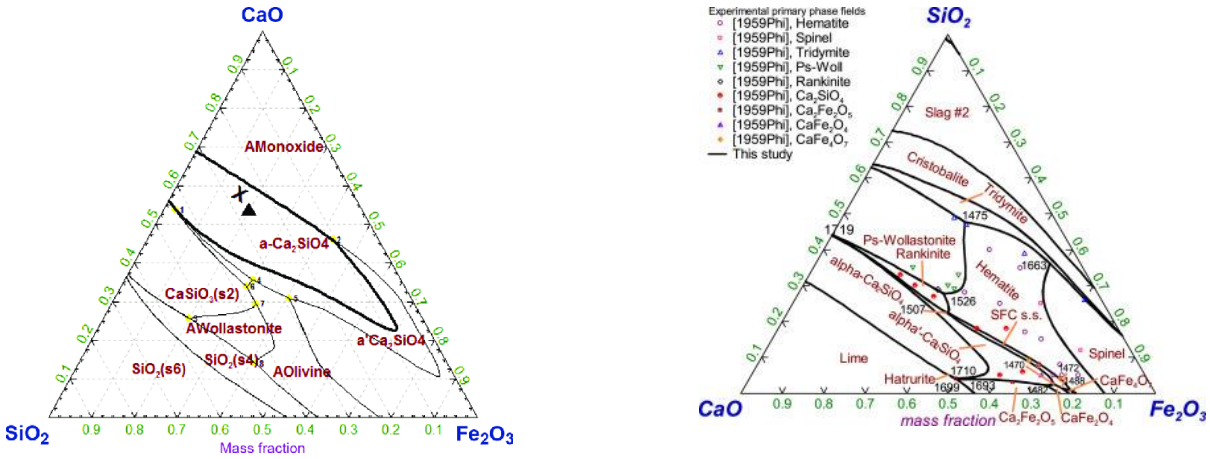

Fig. 4. State diagram ($CaO - Fe_2O_3 - SiO_2$) $(X^B_{12.4} - X^B_{8.4} - X^B_{11.4})$

The most interesting results can be obtained by comparing various properties of the system using methods of modern physicochemical analysis. The fields of the primary phase were experimentally determined and univariant lines in the CaO–FeO–Fe_2O_3–SiO_2 system in air, projected onto the CaO–Fe_2O_3–SiO_2 plane, were calculated. The numbers correspond to the calculated invariant temperatures in K.

The calculated univariant lines and liquidus isotherms at intermediate oxygen partial pressures of 10^{-9} atm, 10^{-8} atm, 10^{-7} atm, 10^{-6} atm and 10^{-5} atm are presented in Fig. 6. Only experimental points with exact or round Lg[$P(O_2)$, atm] are plotted in these figures; further experimental data [5] for other Lg[$P(O_2)$, atm] are not given. Earlier experimental data from Henao et al. [6] were selected for comparison; experimental data from a later paper by Henao et al. [4] were excluded due to inconsistencies found in the data.

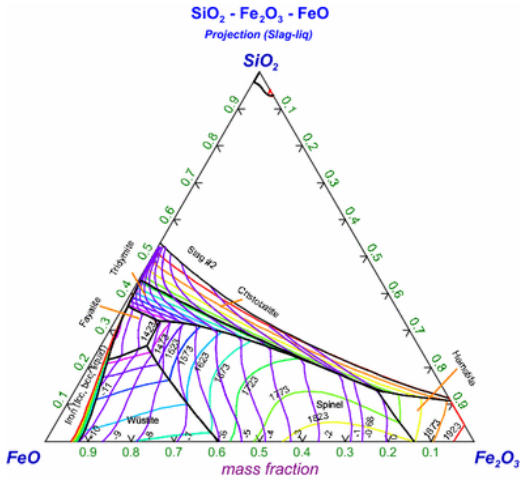

Fig.5. State diagram FeO – Fe_2O_3 – SiO_2

Figure 6 shows the pseudo-ternary phase CaO-FeO-SiO_2 at a partial oxygen pressure of 10^{-9} atm; the field of the primary spinel phase is observed at temperatures below 1481K (1208°C). An increase in the partial pressure of oxygen to 10^{-8} atm and 10^{-7} atm (Fig. 6) leads to an expansion of the field of the primary spinel phase due to the field of the primary wustite phase. At oxygen partial pressures of 10^{-6} atm (Fig. 6) and 10^{-5} atm (Fig. 6), spinel is the only primary phase field observed in the iron oxide corner. An increase in the partial pressure of oxygen also leads to stabilization of the field of the primary pseudowollastonite phase relative to the field of the primary wollastonite phase.

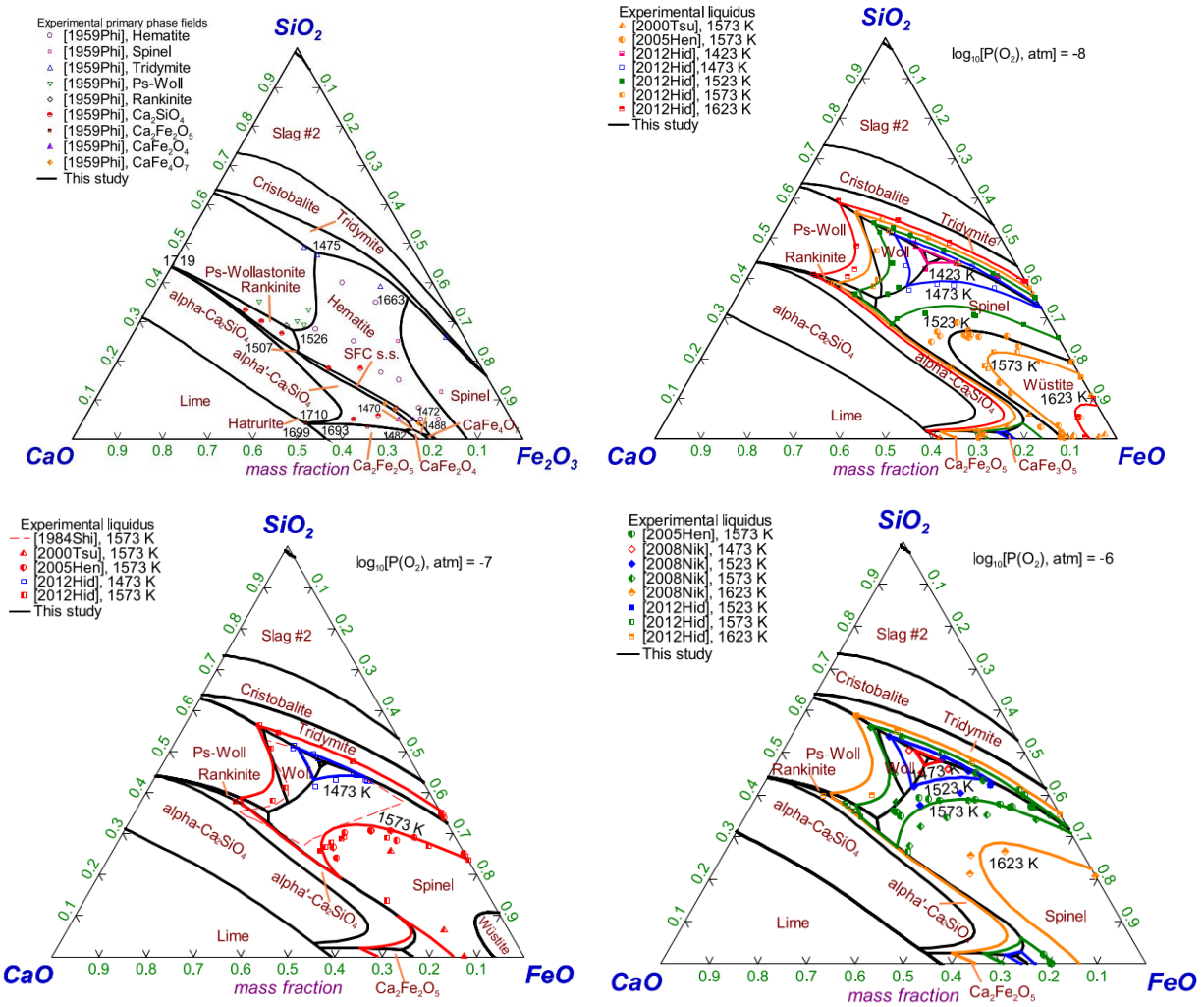

Fig 6. State diagram CaO – FeO – Fe_2O_3 – SiO_2 different SiO_2 content and temperature

Figure 6 shows the presence of fields of the primary phase of olivine and clinopyroxene in a narrow range of compositions. At 1473 K (1200°C) and $P(O_2)=10^{-9}$ atm at the edge of the primary spinel phase field, the phase ensemble Liquid + Spinel + Olivine is predicted by the model parameters, while the phase ensemble Liquid + Spinel + Ca_2SiO_4 is predicted reported by Hidayat et al. [6]. The parameters of the present model appear to overestimate the field stability of the primary olivine phase. There are no experimental works at temperatures below 1473 K (1200 °C) at $P(O_2)$ = 10^{-9} atm and, therefore, there is no experimental data confirming the presence of the field of the primary phase of clinopyroxene, presented in Fig. 6.

Liquidus isotherms at these intermediate oxygen partial pressures are optimized primarily based on experimental data presented by Tsukihashi & Kimura (2000) and Hidayat et al. (2017), which use the equilibration-quench-EPMA method, a reliable and accurate method for determining compositions liquidus and solidus. In general, experimental data on liquidus (Shishin et al., 2019) are well described. Since the liquidus composition of spinel is sensitive to temperature, some of the calculated liquidus compositions in the field of the primary phase of spinel do not fully correspond to experimental data. The slope of the spinel liquidus is almost gentle; therefore, a relatively small change in temperature will lead to a significant change in the composition of the liquidus.

Conclusion

A complete critical re-evaluation of all available phase diagrams and thermodynamic data for the CaO–FeO–Fe2O3–SiO2 system was carried out and a database containing optimized model parameters was obtained. A wide range of experimental data is reproduced within experimental error using a small number of model parameters. In particular, the liquidus is reproduced in a wide range of oxygen partial pressures from

saturation with metallic iron to pure oxygen, including intermediate lg[P(O_2), atm] = $^{-9, -8, -7, -6}$ and $^{-5}$. On the calculated liquidus projection in air, the SFC phase appears for the first time, which is of paramount importance for the agglomeration of iron ores. The present thermodynamic optimization was carried out as part of a broader research program aimed at fully characterizing phase equilibria and thermodynamic properties, followed by the development of a thermodynamic database for the Al-Ca-Cu-Fe-Mg-Si-O-S multi-component system.

Cite this article as: Khursanov A., Hasanov A., Tolibov B. (2023). Physical Properties of Liquid Slag, their Influence on the Basic Parameters of Technological Processes. *Challenges of Science*. Issue VI, 2023, pp. 225-232. https://doi.org/10.31643/2023.26

References

Hasanov A.S. (2003). Physical chemistry of copper production. Navoi. 23 p.

Hidayat, T., Shishin, D., Decterov, S. A., & Jak, E. (2017). Critical thermodynamic re-evaluation and re-optimization of the CaO–FeO–Fe_2O_3–SiO_2 system. Calphad, 56, 58–71. https://doi.org/10.1016/j.calphad.2016.11.009

Kenzhaliyev B. (2019). Innovative technologies providing enhancement of non-ferrous, precious, rare and rare earth metals extraction. Kompleksnoe Ispolzovanie Mineralnogo Syra = Complex Use of Mineral Resources, 310(3), 64–75. https://doi.org/10.31643/2019/6445.30

Shishin, D., Hidayat, T., Fallah-Mehrjardi, A. et al. (2019). Integrated Experimental and Thermodynamic Modeling Study of the Effects of Al2O3, CaO, and MgO on Slag–Matte Equilibria in the Cu-Fe-O-S-Si-(Al, Ca, Mg) System. J. Phase Equilib. Diffus. 40, 445–461. https://doi.org/10.1007/s11669-019-00716-0

Shmonin Y.B. (1981). "Pyrometallurgical depletion of non-ferrous metallurgy slags" M. "Metallurgy", p.130.

Tsukihashi F., Kimura H. (2000). Phase Diagram for the CaO-SiO_2-FeO_x System at Low Oxygen Partial Pressure, in: S. Seetharaman, D. Sichen (Eds.).

Vanyukov A.V., Zaitsev V.L. (1967). "Slags and mattes of non-ferrous metallurgy." M. "Metallurgy", p. 405.

Yessengaliyev D., Baisanov A., Dossekenov M., Kelamanov B., & Almabekov D. (2022). Thermophysical properties of synthetic slags of the FeO – MnO – CaO – Al_2O_3 — SiO_2 system. Kompleksnoe Ispolzovanie Mineralnogo Syra = Complex Use of Mineral Resources, 323(4), 38–45. https://doi.org/10.31643/2022/6445.38